THE FORMATION OF MICROEMULSION AT FLOW CONDITIONS IN ROCK

M. Ruecker[1,2], W.-B. Bartels[1,3], E. Unsal[1], S. Berg[1], N. Brussee[1], A. Coorn[1], A. Bonnin[4]

[1] Shell Global Solutions International B.V., 2288 GS Rijswijk, NL
[2] Department of Earth Science and Engineering, Imperial College London, SW7 2AZ UK
[3] Earth Sciences department, Utrecht University, 3584 CD Utrecht, NL
[4] Swiss Light Source, Paul Scherrer Institute, CH-5232 Villigen, Switzerland

This paper was prepared for presentation at the International Symposium of the Society of Core Analysts held in Vienna, Austria, 27 August – 1 September 2017

ABSTRACT

Surfactant flooding is a chemical enhanced oil recovery (cEOR) technique where low concentrations of surfactant are added to the injection water. The surfactant reduces the oil/brine interfacial tension which, in return, increases the capillary number favoring the viscous mobilization of (capillary) trapped oil. In order to reduce the residual oil saturation significantly, ultra-low interfacial tension ($<10^{-2}$ mN.m^{-1}) between crude oil and aqueous phase is required. That is achieved by employing surfactants that solubilizes the oil and form a microemulsion phase. How low interfacial tension can become depends on the phase behaviour of the surfactant/oil/water system which is often studied with equilibrium phase behaviour tests. However, oil recovery is a dynamic process, and microemulsion formation occurs in situ over different time and length scales depending on the flow and porous medium characteristic.

In this study, we investigated in-situ formation of microemulsion and production of oil by solubilization in a core sample. The aqueous solution of an EOR surfactant was injected into the core sample after the waterflood to solubilize the remaining oil. The surfactant was an internal olefin sulfonate (IOS), and had affinity to the oil phase (n-decane); in situ microemulsion formation occurred. The oil phase was doped with iodo-decane as contrast agent, which allowed visualization of the oil-and emulsion phases using X-ray computed micro-tomography technique. The resolution was sufficient to visualize pure and emulsified oil within individual pores. Image analysis of the scans showed that the emulsification during flow took place at shorter time scales than what was observed at static conditions. These results were consistent with findings of micromodel experiments.

INTRODUCTION

It is commonly accepted that residual oil saturation after conventional waterflood can be further reduced by increasing the capillary number [1-4] $N_c = u\eta/\sigma$ (u is the flow rate, η the viscosity of the injected fluid and σ the interfacial tension (IFT) between the oleic and aqueous phase) as illustrated in Figure 1A [4,12]. Various injection strategies have been developed to enhance the oil recovery (EOR) by changing the properties of the injected

fluid in order to increase N_c. To significantly reduce the residual oil saturation an increase in N_c by several orders of magnitude compared to waterflooding may be required. This can be achieved by surfactants that produce an ultra-low IFT ($<10^{-2}$ mNm^{-1}) between crude oil and the displacing aqueous phase [3,5]. These surfactant systems typically form microemulsions where the surfactant solubilizes some of the oil phase [3,5,8]. In general, the emulsification is studied under controlled conditions such as in laboratory, and facilitated by some form of external mechanical energy, i.e. stirring [6]. But in subsurface applications the emulsification occurs in-situ and application of an external energy is not possible. It is commonly expected that for appropriate composition of surfactants and fluids ultimately a microemulsion will form. What is not clear how long this process will take in absence of "stirring" under in-situ flow conditions which are mostly laminar. There is coupling between emulsification and flow; flow dynamics promote the mixing required for the emulsification while resulting (micro)emulsion properties like increase in viscosity and ultralow IFT impact the flow. Microemulsions can consist of structures with feature sizes – a few nm to several 100 nm – which can increase viscosity and can be larger than the pores of the porous medium (Figure 1C) [6]. IFT reduction will increase the N_c and promote displacement, but a higher viscosity may lead to other adverse effects like trapping and bypassing. For example, Figure 1B shows the viscosities of the microemulsion of n-decane and surfactant solution over a range of salinities used in this study. The equilibrium microemulsion viscosity was 4-6 cP, while the surfactant solution viscosity was ~1 cP and the n-decane viscosity was 0.85 cP [7].

Conventional assessment of the effectiveness of surfactants

To assess the oil recovery efficiency of surfactants, typically equilibrium phase behavior tests are performed. In these tests, the surfactant solution and the oil are initially mixed in test tubes by rigorous shaking, and let stagnate while the emulsification takes place which took approximately 1h for the surfactant/oil/water system used in this study [7,8]. The properties of the microemulsion are then assessed by visually inspecting the solubilization, measuring the oil/water IFT and the viscosity of the resulting microemulsion to determine the optimum surfactant solution [8]. These tests are done under static conditions and do not probe the influence the flow and in-situ mixing.

Pore-scale studies on surfactant flooding

Glass micromodels allow direct visualization of the pore space, and provide crucial information to understand the fundamentals of the pore-scale physics which play a role in the emulsification. Studies in micromodels have shown that the microemulsions can form in situ under flowing conditions at shorter time scales than in static conditions [7]. However, the pore structure of a rock is more complex, and, therefore, may have significant influence on the emulsification behaviour. Coreflood experiments can be performed where the aqueous solutions of surfactant are injected in an oil-saturated rock of several centimeters to 1m length [2,3]. These experiments provide an estimate on the average oil recovery values but do not give access to microscopic details at pore scale.

Recent advances at μCT synchrotron beamlines have enabled to study multiphase flow through rock samples at a time resolution of few seconds [9][10]. With this technique also

the effect of surfactant has been studied, however, the surfactant/oil/water system did not form microemulsions with ultralow interfacial tension [11] .

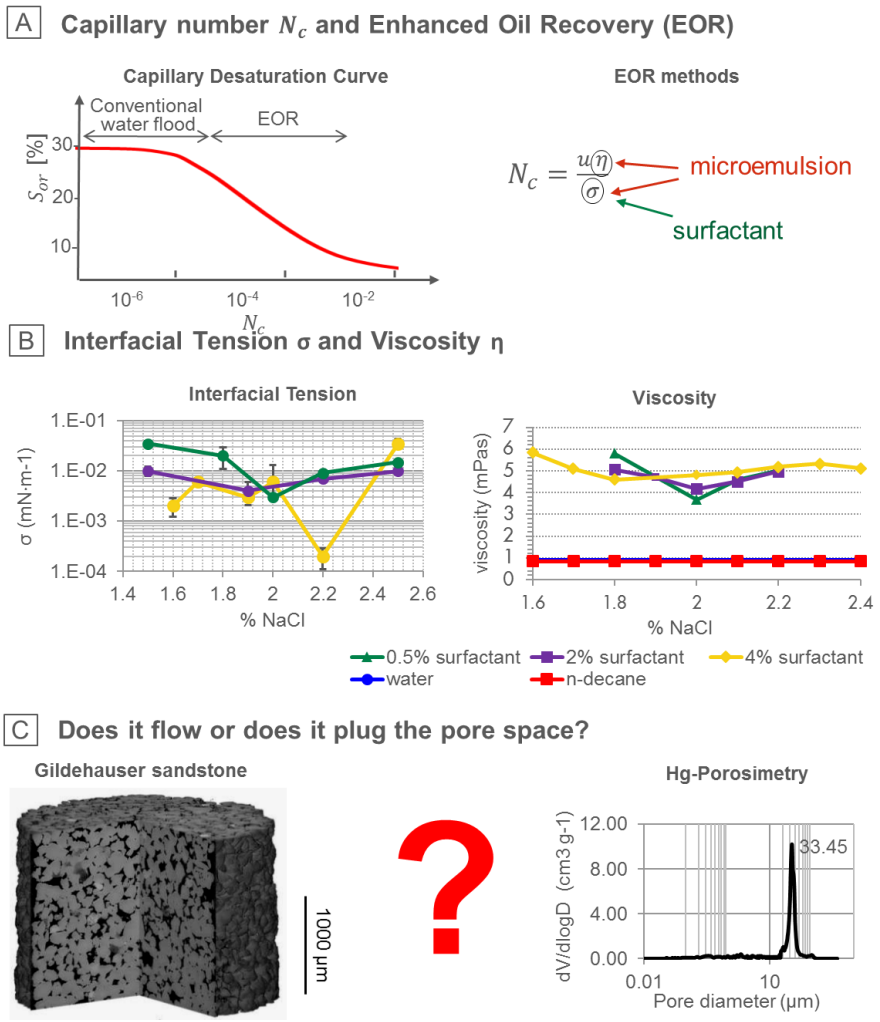

Figure 1: Capillary desaturation curve (A-left: adapted from Lake, 1989 [1]) and capillary number formulation (A-right). IFT and viscosity values of microemulsions in the behavior study (B: adapted from Unsal et al., 2016 [7]). C: flow dynamics in pore space depend on the topology, pore size distribution and feature size of microemulsions.

Here, we present a coreflood experiment using fast X-ray computed micro-tomography. We studied the in-situ emulsification of oil during surfactant flooding. The resolution was enough to visualize pure and emulsified oil which provided a more detailed insight into the time and length scales associated with the in-situ emulsification.

MATERIALS AND METHODS

Sample selection and preparation

Water-wet Gildehauser sandstone was used as the rock sample [10]; its properties are listed in Table 1. The corresponding pore size distribution obtained by Hg-porosimetry is

displayed in Figure 1C. The sample was cleaned and embedded into polycarbonate by heat-shrinking. Prior to the coreflood, the sample was saturated with brine which was then displaced by drainage with oil (n-decane). The oil phase was doped with iodo-decane as a contrast agent (22% iodo-decane / 78% decane).The brine composition is given in Table 2.

Table 1. Core sample details.

Core material	Porosity	Permeability	Core length	Core diameter
Gildehauser sandstone	0.2	1 Darcy	20 mm	4 mm

The surfactant solution consisted of 1% Na_2CO_3, 5% 2-butanol, 1.25% NaCl and 2% surfactant. It was chosen based on its capability to form microemulsions with n-decane at ambient conditions. The surfactant was an internal olefin sulfonate (IOS) with 20-24 carbon atoms (C20-24) and is produced by Shell Chemicals as the ENORDET O series.

Table 2. Brine composition,

Ion	Na^+	K^+	Mg^{2+}	Ca^{2+}	Cl^-	Ionic Strength [mol/L]	pH
FW [mg/L]	4270	7240	20	300	13750	0.396	7

Beamline based fast X-ray computed micro-tomography

The experiments were performed at the TOMCAT beamline of the Swiss Light Source (Paul Scherrer Institute). The fast synchrotron-based X-ray computed micro-tomography facility enabled us to collect a full 3D scan (1500 projections) of a region of interest (ROI: 1400x1400x900 voxels with a pixel size of 3 μm) located 2mm above the inlet in 7s. A white beam with 5%, 250 um Al was used.

The core samples were mounted vertically in a flow setup containing two remotely controlled piston pumps [13], which enabled a continuous rotation for 4D tomography. The injection was done at the bottom of the sample. The injection rate was 30 $\mu l.min^{-1}$ for both floods, and corresponded to a interstitial velocity of approximately 12 $mm.min^{-1}$ or 1.68 pore volume per minute. The corresponding capillary number was $N_c = 1.1 \times 10^6$. The experimental protocol started with sample saturated with oil after primary drainage. Two consecutive injections were performed; waterflood followed by the surfactant injection. The waterflood was imaged taking a scan at 1 scan at every 7s and surfactant flood was imaged at 1 scan every minute.

Image processing

The images obtained from the beamline were reconstructed using the Paganin method [14,15]. They were then filtered, segmented and processed with Avizo 9.0 (FEI) and Matlab (MathWorks) [10]. Rock, initial water and oil phases were segmented during the conventional waterflood. During the surfactant flood the mixing with remaining oil led to the formation of emulsions with a range of composition and associated of grey levels ranging between (un-doped) water to doped oil levels. The degree of emulsification was assessed from the grey level. In addition to the coreflood images, equilibrated phase

behaviour test tubes were also scanned in a benchtop µCT-scanner Xradia (Zeiss) in order to study the composition of the (fully) equilibrated middle microemulsion phase.

RESULTS

Phase behaviour studies (static)

Based on equilibrium phase behavior analysis of the surfactant solution and n-decane, the optimum salinity was at 1.25% NaCl. Since the oil was doped with iodo-decane, the phase behaviour tests were repeated with the doped n-decane, which did not affect the optimum salinity (Figure 2A).

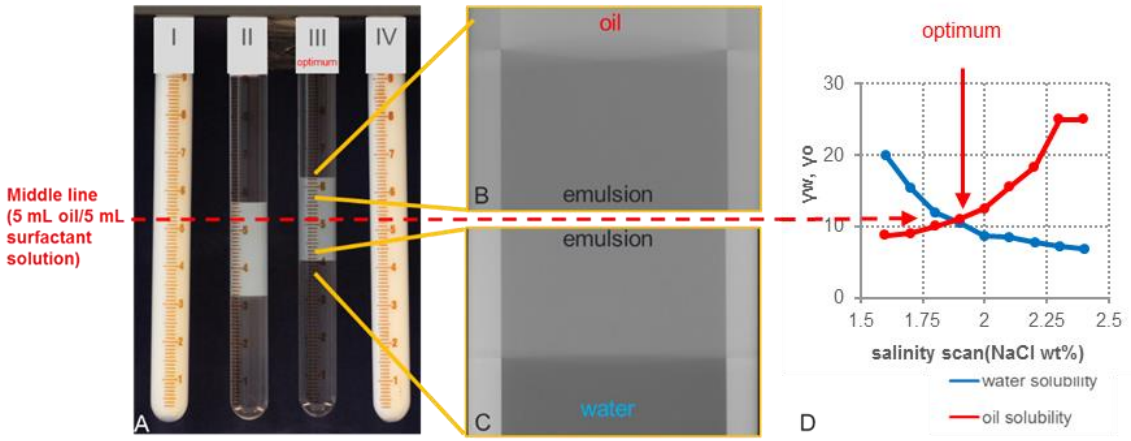

Figure 2: (A) Equilibrium phase behaviour tests of the surfactant/oil/water system used in this study with I: 0.75% NaCl II: 1%NaCl, III: 1.25% NaCl (optimum) and IV:1.5%NaCl. (B+C) exact composition of tube III was further analysed with uCT scanning. Based on the grey values of the image an oil content of 53% and water content of 47%, (D) solubility of the surfactant in oil and aqueous phases for the studied system [7,8].

The 1.25% NaCl test tube was scanned in the µCT-scanner; the oil (top layer), aqueous (bottom layer) and the microemulsion (middle layer) each had a distinctly different grey value (Figure 2B). The aqueous and oil phase content of the microemulsion was estimated using the linear blending rule for X-ray attenuation coefficients expressed here as

$$Gray\ value\ (emulsion) = \gamma_o\ Gray\ value\ (oil) + \gamma_w Gray\ value\ (water), \qquad (1)$$

where the oil and water content of the emulsion are γ_o and γ_w, respectively. Based on the grey values of the image of the middle emulsion phase, an oil content of 53% and 47% of the surfactant solution was determined. The test tubes contained a 1:1 ratio of aqueous and oil phases (5mL surfactant solution + 5mL n-decane). At the optimum salinity, the microemulsion was expected to contain 50% aqueous solution and 50% oil phase because the surfactant had similar affinities to the oil and the water. Figure 2D shows the solubility diagram of the surfactant/oil/water system which was obtained by analysing the phase behaviour tubes shown in Figure 2A [7]. It showed that the surfactant had similar solubility in the aqueous and oil phases at the optimum salinity. The values extracted from the µCT-

scanner images indicated that the microemulsion at the optimum salinity, indeed, contained approximately equal volumes of aqueous and oil phases.

In situ formation of microemulsion in rock

Figure 3B shows the oil (grey) and water phase (black) at the end of waterflood and Figure 3C shows the first scan of the surfactant injection 7s after the injection started. At this time, the total injected surfactant solution volume was less than 1PV (~0.8 PV), but it is likely that surfactant breakthrough occurred through preferential pathways and/or quasi-miscible flow and associated fingering [12]. Furthermore, the scan was taken 2mm above the inlet; the surfactant solution has already passed through this segment at 7 s. Figure 3D shows the final scan of the surfactant flooding which was taken approximately 45 mins later. The pore space was flooded by the surfactant for multiple PVs, and it was assumed that any additional displacement due to quasi-miscible was completed. Compared to the first scan with the surfactant, there were subtle differences in the saturation profile; difference in grey levels in the bigger pores were directly visible (compare Figure 3C and 3D).

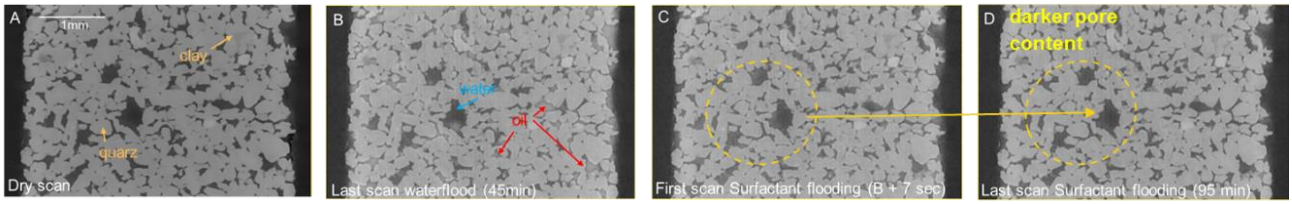

Figure 3: (A) Grey scale image of the sample without any fluid, (B) Last scan of the waterflood: oil-phase appears bright and the water phase dark, (C) 7 s after surfactant flood started, (D) Content of large pores become slightly darker.

The scans taken during the waterflood and surfactant flood were processed for detailed saturation profiles. For improved signal-to-noise ratio, volume averaged grey levels were considered. Corresponding to Equation (1) this averaged grey value of the pore space indicates the composition of the fluid. In Figure 4A the volume averaged grey value over the pore space of each image vs. time is displayed. The total grey value of each slice as a function of vertical position was extracted from the images during the surfactant-flood (Figure 4B). In combination with the oil-saturation obtained from the waterflood, a linear correlation of the oil-saturation and the grey value was determined and used to estimate the oil-content in the pore space during the surfactant flood. Based on this estimation after the surfactant flood around 16% of the oil remained in the core in form of emulsion. Shortly after the surfactant injection started, the oil saturation decreased sharply from 40% to 18%. This sharp reduction suggested that the surfactant was transported quickly, and it covered most of the oil/water interface almost immediately. From these images, it is not possible to infer the emulsification rate, however, it is likely that the IFT reduction was enough to mobilize a relatively significant amount oil in seconds. As the surfactant injection continued, the oil saturation gradually decreased a further 2%, and the residual oil saturation reached 16% (Figure 4B, at 95 mins). During this injection period, the pore space was flooded by the surfactant already for many PVs, and surfactant solubilized over time of the trapped oil (Figure 4C).

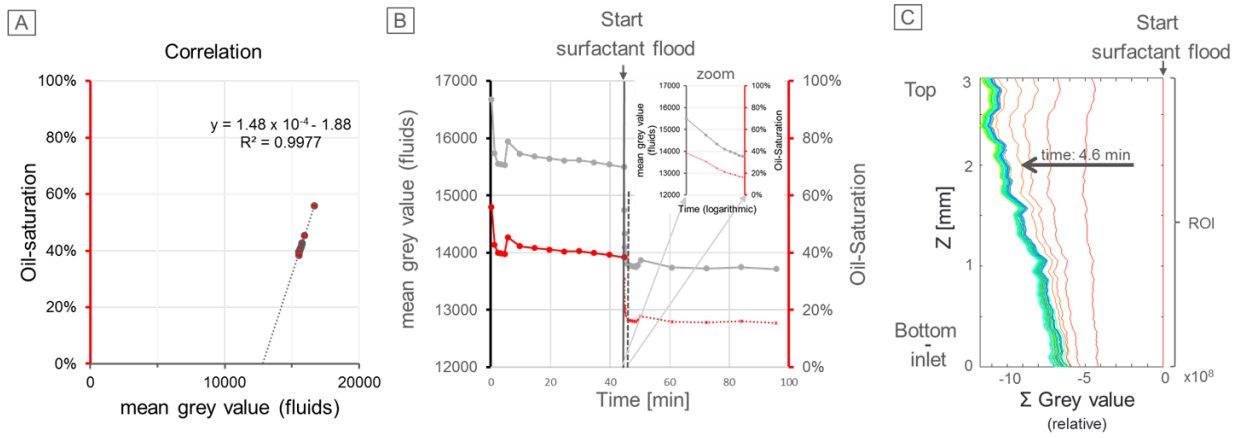

Figure 4: (A) Correlation between the oil saturation computed based on the segmented image and the mean grey value of the fluid phases.(B) Oil saturation vs time (red solid line) for the waterflood imbibition. Total grey value (grey) was used to estimate the oil-content during the surfactant flood (red dashed line). (C) Change of the grey-scale value during the surfactant flood along the z axes is shown relative to the first scan.

Pore-scale processes

The grey value analysis of the images was then used for understanding the pore-scale behavior of the in-situ emulsion formation and quasi-miscible flow. In Figure 5, images from waterflood and surfactant flood are shown. The color-scheme from violet to red highlighted the difference in grey values inside the pore space. Figure 5A was taken at the end of waterflood where the oil is red and the water is blue. Figure 5B shows the scan which was taken 7s after the surfactant flooding started. The initially oil filled (red) pores already changed composition: the color changed from light to dark blue which suggested presence of an aqueous phase, but possibly with different water content, i.e. emulsion with oil solubilized. At the end of the surfactant flooding, the fraction of the dark blue within individual pores increased (Figure 5C). After flooding the sample with the surfactant solution for many PV, the surfactant accessed and solubilized most of the trapped oil. However, it was not possible to mobilize all of the solubilized oil even after that many pore volumes of continuous surfactant injection.

The fact that the surfactant accessed and mobilized a significant potion of the remaining oil during the initial few seconds (Figure 5B) suggested that the emulsification rate was much quicker compared to rates observed at static conditions. Unsal et al. (2016) [7] observed that microemulsion formed faster under dynamic conditions in pore space than expected from static phase behaviour studies. In micromodel experiments, the diffusion controlled processes as in dead end pores (Figure 5C) and turbulence mixture during co-injection of two fluids (Figure 5D) provided the means for stirring and quicker emulsification. Their effects may be even more pronounced in a core as the connectivity in a 3D porous system is significantly higher than in a 2D system such as a microfluidic chip.

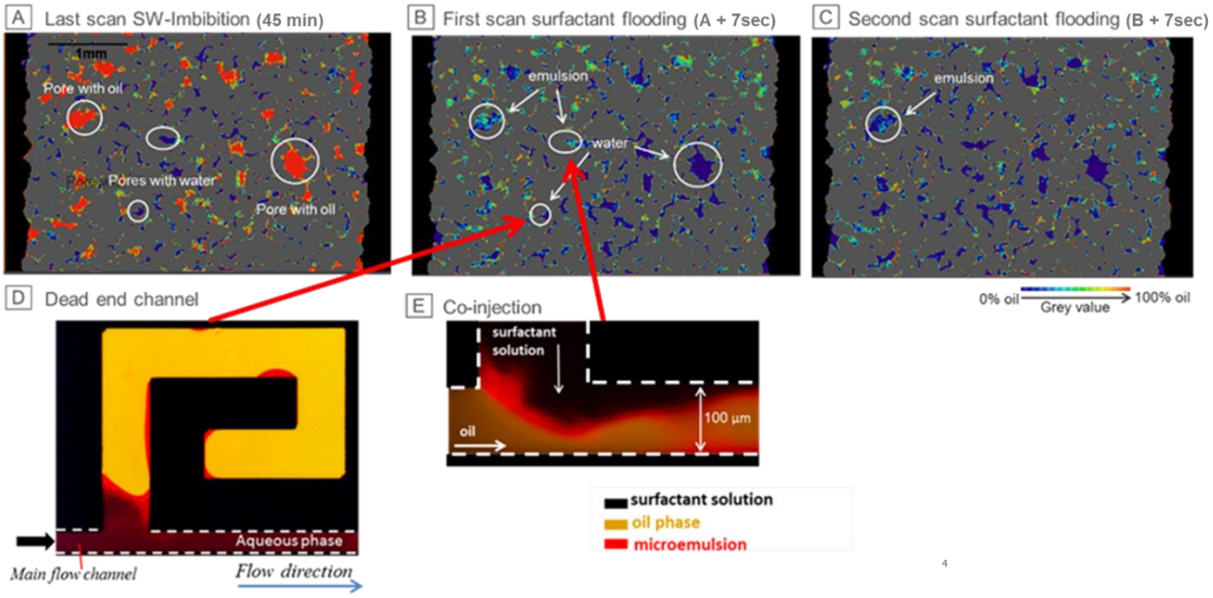

Figure 5: (A) Last scan of the waterflood-imbibition, displaying the oil-(red) and water (blue) distribution, (B) Image of first scan during surfactant flooding showing the rock and the grey values in the pore space in a color-scheme to highlight the variety. (C) Further oil solubilisation during surfactant flooding, (D)Dynamic phase behavior experiments in micromodels [7].

CONCLUSION

In this study, we conducted a flow experiment with surfactant/oil/water system in a rock sample whilst imaging with fast µ-CT. We used a surfactant which formed microemulsions in presence of n-decane, and allowed the visualization of quasi-miscible flow and oil recovery by solubilisation. The resolution within individual pores was sufficient to identify 'pure/clean' and 'emulsified' oil. The image analysis of the images taken from the experiments suggested that the emulsification during flow took place at shorter time scales (seconds) than what would be expected at static conditions. It is probable that the diffusion of surfactant and mixing due to flow in the confined pore space facilitated this relatively faster emulsification rates.

ACKNOWLEDGEMENTS

We acknowledge the Paul Scherrer Institut, Villigen, Switzerland for provision of synchrotron radiation beamtime at beamline Tomcat of the SLS and would like to thank F. Marone and M. Stampanoni for their support.

REFERENCES

1. Lake, L. W. ,1989, *Enhanced Oil Recovery*. Prentice Hall: Upper Saddle River, NJ.
2. Putz, A., Chevalier, J. P., Stock, G., Philippot, J., 1981, A Field test of microemulsion flooding, Chateaurenard Field, France. *JPT, J. Pet.Technol. 1981, 33*, 710−718.
3. Hirasaki, G. J., Miller, C. A., Puerto, M., 2011, Recent advances in surfactant EOR. *Soc. Pet. Eng. Journal* 16, 889−901.
4. Dullien, F. A., & Brenner, H., 1991, *Porous Media: Fluid Transport and Pore Structure* (2 ed.). San Diego Calif.: Academic Press.
5. Salager, J. L., Bourrel, M., Schechter, R. S., Wade, W. H., 1979, Mixing rules for optimum phase behavior formulations of surfactant/oil/water systems. *SPEJ, Soc. Pet. Eng. J.*, 19, 271−277.
6. Sjoblom, J., 1996, *Emulsions and emulsion stability*, Mercel Dekker, New York.
7. Unsal, E., Broens, M., & Armstrong, R. T., 2016, Pore Scale Dynamics of Microemulsion Formation. *Langmuir*, 32(28), 7096-7108.
8. Huh, C., 1979. Interfacial tensions and solubilizing ability of a microemulsion phase that coexists with oil and brine. *Journal of Colloid and Interface Science*, 71(2), pp.408-426.
9. *Proceedings of the National Academy of Sciences*, 110(10), 3755–3759.
10. Rücker, M., Berg, S., Armstrong, R.T., Georgiadis, A., Ott, H., Schwing, A., Neiteler, R., Brussee, N., Makurat, A., Leu, L. and Wolf, M., 2015. From connected pathway flow to ganglion dynamics. *Geophysical Research Letters*, *42*(10), pp.3888-3894.
11. Youssef, S., Rosenberg, E., Deschamps, H., Oughanem, R., Maire, E., Mokso, R., 2014, Oil Ganglia Dynamics in Natural Porous Media During Surfactant Flooding Captured by Ultra-Fast X-Ray Microtomograpy, Paper SCA2014-023 presented at the SCA International Symposium, Avignon, France, 8–11September.
12. Lenormand, R., Toubul, E., Zarcone, C. Numerical models and experiments on immiscible displacements in porous media. *Journal of Fluid Mechanics*, 1988, 189, 165-187.
13. Armstrong, R., Ott, H., Georgiadis, A., Rücker, M., Schwing A., Berg, S., 2014, Subsecond Pore-Scale Displacement Processes and Relaxation Dynamics in Multiphase Flow. *Water Resources Research*, 50(12), 9162–9176.
14. Paganin, D., Mayo, S., Gureyev, T., Miller, P., and Wilkins, S.,2002, Simultaneous Phase and Amplitude Extraction from a Single Defocused Image of a Homogeneous Object. *Journal of Microscopy*, 206(1), 33–40.
15. Marone, F., Stampanoni, M., 2012, Regridding Reconstruction Algorithm for Real-Time Tomographic Imaging. *Journal of Synchrotron Radiation*, 19, 1029–1037.